Model of a Microtoroidal Magnetometer

S. Forstner[a], J. Knittel[a], H. Rubinsztein-Dunlop[a] and W. P. Bowen[a]

[a]School of Mathematics and Physics, University of Queensland, St Lucia, Queensland 4072, Australia

ABSTRACT

We present a model of a cavity optomechanical magnetic field sensor based on a microtoroidal resonator. The magnetic field induced expansion of a magnetostrictive material is transduced onto the physical structure of a highly compliant optical microresonator. The resulting motion is read out optically with ultra-high sensitivity. According to our theoretical model sensitivities of up to 750 fT/$\sqrt{\mathrm{Hz}}$ may be possible. The simultaneous presence of high-quality mechanical and optical resonances in microtoroids greatly enhances both the response to the magnetic field and the measurement sensitivity.

Keywords: cavity optomechanics, magnetic field sensors, magnetostriction, integrated microcavity, microtoroid

1. INTRODUCTION

Ultra-sensitive magnetometers are indispensable for a wide range of practical applications.[1] The field is dominated by superconducting quantum interference devices (SQUIDs),[2] which achieve sensitivities of up to one fT/$\sqrt{\mathrm{Hz}}$, allowing the detection of single magnetic flux quanta.[1] However, SQUIDs suffer form major drawbacks: They require cryogenic cooling and they are not suitable for miniaturization ande integration on a chip scale.[3]

Thus, creating ultra-sensitive magnetic field sensors capable of operating at room temperature is an important research goal. On a macroscale, magnetic field measurements with record sensitivities of 160 aT/$\sqrt{\mathrm{Hz}}$ at room temperature can be achieved with spin exchange relaxation-free (SERF) magnetometers.[4] SERF magnetometers measure magnetic fields by monitoring a high density vapor of alkali metal atoms precessing in a near-zero magnetic field.[5] SERFs have been used successfully in various applications including medicine and geology, but also have significant disadvantages. Firstly, they are relatively large with dimensions at least in the mm-range even when using micro-fabricated gas cells.[6] Secondly, they have a low dynamic range and already at geomagnetic fields ($\approx 50~\mu$T) are adversely affected by the non-linear Zeeman effect[2, 7]

Currently there is a large interest in Nitrogen-Vacancy(NV) center based magnetometers, as they overcome the size constraints of SERFs and SQUIDs, being nm to μm size. These devices combine sensitivities reaching 4 nT/$\sqrt{\mathrm{Hz}}$ with room temperature operation, optical readout and small size,[8] and are predicted theoretically to reach the fT/$\sqrt{\mathrm{Hz}}$ range.[9] This has enabled magnetic field imaging,[9] and magnetic resonance imaging[10] at the nanoscale with a single NV center. Three-dimensional magnetic field imaging was demonstrated using a CCD camera to read out an ensemble of NV centers in a macroscopic crystal.[11] However, the wide application of NV centers is hampered by fabrication issues, intricate read-out schemes,[12] misalignment of the magnetic field that prepares the atomic states,[11] and bulky optics required for signal detection.

Magnetostrictive materials provide a possible alternative for miniaturization and integration of room temperature magnetometers. These materials deform under an applied magnetic field, and combined with a sensitive position sensor, provide the basis for a robust and highly sensitive magnetic field sensing technology that does not require cooling, or rely on intricate read-out schemes, and has the potential for miniaturization.

Already in 1989 a fiber interferometer based magnetometer using the magnetostrictive material Metglas achieved a sensitivity of 70 fT/$\sqrt{\mathrm{Hz}}$ at a frequency of 34 kHz. Moreover, the sensor's response to magnetic fields was linear for flux densities up to mT.[13] The magnetostrictive material had a size of several centimeters.

Further author information: (Send correspondence to J.K.)
J.K.: E-mail: j.knittel@physics.uq.edu.au, Telephone: +61 7 33 53412

Today the most commonly used magnetostrictive material is Terfenol-D as, at room temperature, it produces the largest saturation strain on application of a magnetic field of all known materials.[14]

Magnetometers based on Terfenol-D have already been demonstrated by several groups: By creating composite materials combining Terfenol-D layers with piezoelectric materials a sensitivity of 10 pT/$\sqrt{\text{Hz}}$ was demonstrated, and the composite material had a size on the cm-scale.[15] In another experiment optical fiber based Bragg gratings were coated with Terfenol-D. A spectrometer was used to measure the resonance frequency shift of the Bragg grating that was deformed by the expanding Terfenol-D. The authors reported a sensitivity of 0.3 mT.[16] In both applications the sensitivity was ultimately limited by the methods that detected the Terfenol-D induced deformations.

However, the described sensors have dimensions on the order of centimeters and are not suitable for integration on a chip-scale or for fabrication in a 2-dimensional array. Smaller sensors based on Terfenol-D have been demonstrated, and by detecting the deformation of commercial AFM cantilevers that were coated with Terfenol-D, a magnetic field sensitivity of 1 μT was achieved.[17] This shows the ability of Terfenol-D based sensors to be realized on the microscale, however, this particular sensor suffers the major drawback that the achieved sensitivity is insufficient for many applications. Also integration on a chip and production of an array of sensors would be technically very demanding.

In Ref.[18] a first proof of principal demonstration of an optomechanical magnetometer was presented, achieving an experimentally measured sensitivity of 400 nT/$\sqrt{\text{Hz}}$. However, theoretical modeling showed that sensitivities of up to 750 fT/$\sqrt{\text{Hz}}$ may be possible with an optimized microtoroidal sensor. In this letter we present in detail the derivation of the predicted sensitivity using the formal framework presented in Ref.[19] and based on a finite element model.

2. MODEL OF A MICROTOROIDAL MAGNETIC FIELD SENSOR

2.1 Noise sources

The noise spectrum $S_{\Omega\Omega}^{\text{noise}}$ for a cavity optomechanical magnetic field sensor is given by[19]

$$S_{\Omega\Omega}^{\text{noise}}(\omega) = S_{\Omega\Omega}^{\text{therm,q}} + S_{\Omega\Omega}^{\text{meas}} = g^2 \left| \chi_q(\omega) \right|^2 [2m_q k_B T \Gamma_q] + S_{\Omega\Omega}^{\text{meas}}(\omega), \tag{1}$$

where g is the optomechanical coupling constant,[20] $\chi_q(\omega)$ is the mechanical susceptibility of the qth eigenmode of the oscillator, m_q its effective mass and Γ_q its mechanical dissipation rate. The first term $S_{\Omega\Omega}^{\text{therm,q}}$ corresponds to thermal excitation of this eigenmode and the second term $S_{\Omega\Omega}^{\text{meas}}$ accounts for shot and frequency noise on the laser field, and other noise sources such as electronic noise in the detectors used to measure the optical field. We neglect fluctuations of the radiation pressure force δF_{rp},[19] as they cause only a minor perturbation when using optical powers typical for measurements in a toroidal WGM.

Ultimately, the detection of any signal imprinted on the optical field is limited by laser shot noise, which is spectrally flat to a good approximation.[21] We assume a shot noise background of $(S_{\Omega\Omega}^{\text{meas}})^{1/2} = 20$ Hz/$\sqrt{\text{Hz}}$, consistent with experiments.[22]

At the length- and mass-scales of microtoroids, thermal excitation of mechanical modes at room temperature becomes a significant noise source, as a simple example calculation shows: a typical microtoroid with a major radius of $R = 30$ μm and an optical resonance frequency at $\Omega_c = 306$ THz (corresponding to $\lambda_c = 980$ nm) exhibits an optomechanical coupling of $g = \Omega_c/R = 6.41 \cdot 10^{19}$ Hz/m.[20] For a typical radial breathing mode with effective mass $m_q = 10$ ng, mechanical quality factor $Q_q = 10^4$ and resonance frequency $\omega_q = 2\pi \cdot 30$ MHz, the displacement noise $S_{\Omega\Omega}^{\text{therm,q}}$ on resonance at room temperature $T = 300$ K is calculated as

$$\left(S_{\Omega\Omega}^{\text{therm,q}} \right)^{1/2} = g \cdot \chi_q(\omega_q) \cdot F_{\text{therm}} = \frac{g Q_q}{m_q \omega_q^2} \cdot \sqrt{2 k_B T m_q \omega_q Q_q^{-1}} = 71 \frac{kHz}{\sqrt{Hz}} \gg 20 \frac{Hz}{\sqrt{Hz}}, \tag{2}$$

where we have written the mechanical susceptibility in the form $\chi_q = [m_q(\omega_q^2 - \omega^2 - i\Gamma_q \omega)]^{-1}$. Thus the thermal excitation of the mode can easily be measured at room temperature and dominates the noise floor around its resonance frequency. However, the desired signal is enhanced as the mechanical susceptibility $\chi(\omega)$, proportional

to the thermal noise, so that at frequencies around a mechanical mode, the ratio of signal to Brownian noise remains constant, but all other noise sources are suppressed proportional to $\chi(\omega)$. This leads to a higher overall signal-to-noise ratio and thus a higher sensitivity around mechanical eigenmodes.

In addition to the fundamental shot noise, $S_{\Omega\Omega}^{\text{meas}}$ can also comprise other noise sources: thermorefractive noise in a microtoroid stems from localized thermal fluctuations of the refractive index of glass. It increases with lower frequencies and exceeds the laser shot noise in microtoroids below 30 MHz,[22] therefore constituting the dominant noise source for measurements at lower frequencies. Its spectral shape has been theoretically modeled in Ref.[23] In principle it can be minimized by controlling material properties.

Electronic noise is generally not an issue in measurements of the transduced signal, as, using suitable detection electronics, it remains several decibel below the laser shot noise.[22]

At frequencies below one kilohertz, mechanical noise sources such as vibrations in the taper-toroid coupling or in the coupling of a laser beam from free space into fiber have to be considered. These noise sources can however be eliminated by carefully designing the measurement setup.

2.2 Model geometry and FEM simulation

We model a toroidal WGM-resonator which is made of a central Terfenol-D cylinder (radius $\tilde{R} = 24\mu$m, height $H = 5\mu$m) with a surrounding silica torus (major radius $R = 30\mu$m, minor radius $R' = 3\mu$m) (see Fig. 2). For the mechanical resonator, this yields a total mass of

$$M = \rho_{\text{Terfenol}} \cdot \pi \tilde{R}^2 H + \rho_{\text{Silica}} \cdot 2\pi R R'^2 = 88\text{ng}, \tag{3}$$

where we have used the densities of Terfenol and silica, $\rho_{\text{Terfenol}} = 9.25 \text{ g/cm}^3$,[14] and $\rho_{\text{Silica}} = 2.65 \text{ g/cm}^3$,[24] respectively. The torus is made of silica and constitutes the optical resonator (see Fig. 2). We assume that the system vibrates in a single mechanical radial breathing mode with $Q_q = 1000$.[20] A finite element simulation (COMSOL) yielded the eigenfrequency $\omega_q = 2\pi \cdot 5.6$ MHz and effective mass $m_q = 16$ ng (see Fig. 1). Applying the theory developed in Ref.[19] to this model, we can calculate the minimum detectable magnetic field as a function of frequency

$$\frac{|\vec{B}|^{\text{min}}(\omega)}{\sqrt{\text{RBW}}} = \frac{1}{c_{\text{act}}} \sqrt{2k_B T M \Gamma_q + \frac{M}{m_q} \frac{S_{\Omega\Omega}^{\text{meas}}}{g^2 |\chi_q(\omega)|^2}} \tag{4}$$

$$= \frac{1}{c_{\text{act}}} \sqrt{2k_B T M \Gamma_q + g^{-1} S_{\Omega\Omega}^{\text{meas}} M m_q \cdot (\omega_q^2 - \omega^2 - i\Gamma_q \omega)}, \tag{5}$$

where RBW is the resolution bandwidth of the measurement (i.e. the inverse of the measurement time). The magnetic actuation constant c_{act} determines the strength of the coupling between applied magnetic field and effective force on the mechanical oscillator.

It can be seen that, in the usual limit where the radiation pressure force due to photon number fluctuations is negligible, a high mechanical quality factor $Q_q = \Gamma_q/\omega_q$ is always advantageous for precise sensing, reducing the thermal noise, and also, on resonance, the effect of the measurement noise through its contribution to $\chi_q(\omega) = [m_q(\omega_q^2 - \omega^2 - i\Gamma_q \omega)]^{-1}$.

In this limit, a low effective mass is beneficial for sensing, as its total effect will be a suppression of the measurement noise. Also improving the optical quality factor of the cavity is of advantage, as common measurement techniques convert a frequency shift signal to an amplitude- or phase-signal, which is enhanced as Q_{opt} relative to the measurement noise.

In the following sections, we calculate the magnetic actuation constant c_{act} of the model and then discuss its predicted performance.

2.3 Magnetic actuation constant c_{act}

The following paragraphs are dedicated to the calculation of the magnetic actuation constant c_{act} via finite element modeling. It is given by the spatial overlap of the force distribution $\vec{f}_{\text{MS}}$ created by the magnetostrictive medium and the modeshape function $\vec{\Psi}_q(\vec{r})$.[19]

$$c_{\text{act}} = \frac{1}{B} \int_V \vec{f}_{\text{MS}}(\vec{r}, t, B) \cdot \vec{\Psi}_q(\vec{r}) d^3 r, \tag{6}$$

where B is the magnitude of the applied magnetic field. We approximate the displacement amplitude for a radial breathing mode as proportional to the radial coordinate, $\vec{\Psi}_q(\vec{r}) \propto \vec{r}$. This is a good approximation for this particular system, as confirmed by finite element simulation (see Fig. 1). In a straightforward calculation, the normalization condition $\int_V \left| \vec{\Psi}_q(\vec{r}) \right|^2 d^3 r = V$ finally yields

$$\vec{\Psi}_q(\vec{r}) = \frac{\sqrt{2}}{R} \vec{r}. \tag{7}$$

The displacement $\vec{\Psi}_q(\vec{r})$ is radially symmetric and proportional to the distance from the center of the oscillator. In order to evaluate the integral on the right hand side of Eq. (6), we still need to calculate the magnetostrictive
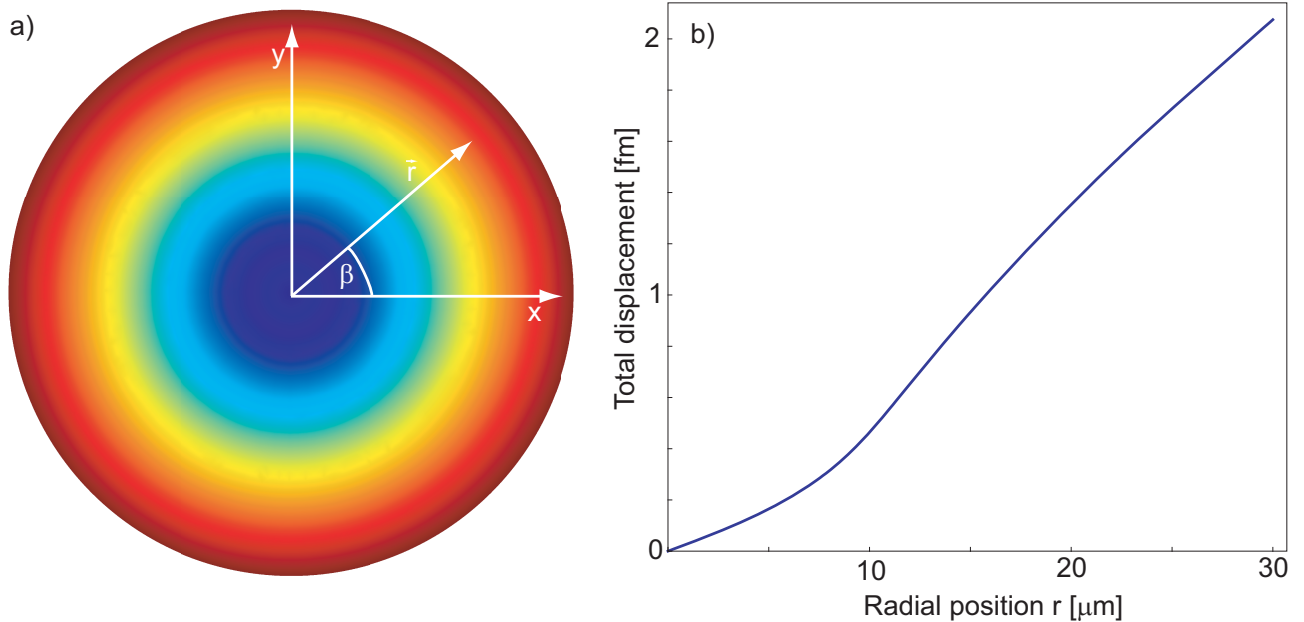

Figure 1. (color online) a) Top view on a simulated radial breathing mode of the described model with color-coded displacement amplitude exhibiting radial symmetry. b) The displacement amplitude plotted against the radial coordinate is approximately linear in its radial position.

force density $\vec{f}_{\text{MS}}$. It is given by the divergence of the stress tensor $\bar{\sigma}(\vec{r}, t)$[25]

$$\vec{f}_{\text{MS}}(\vec{r}, t, \vec{B}) = \vec{\nabla} \cdot \bar{\sigma}(\vec{r}, t). \tag{8}$$

The stress created by a magnetostrictive material in an uniform magnetic field $\vec{B}$ is in the most general case given by $\vec{\sigma}(\vec{r}, t) = \vec{B}\bar{\alpha}$, where $\bar{\alpha}^B$ is the magnetostrictive stress tensor.[26] However, in a magnetostrictive material with aligned domains, as considered here, only the *longitudinal* magnetostrictive stress coefficient α_{33}^B is of interest.[14] The magnetostrictive normal stress is then

$$\vec{\sigma}(\vec{r}, t) = B(t)\hat{e}_x \cdot \alpha_{3x}^B(\vec{r}), \tag{9}$$

where $\alpha_{3x}^B(\vec{r})$ is the projection of the longitudinal magnetostrictive stress on the direction $\hat{e}_x$ of the magnetic flux density B. Using the equality $\alpha_{3x}^B(\vec{r}) = \alpha_{33}^B(\vec{r})\cos\theta$, where θ denotes the angle between the direction of the magnetic field and the main magnetisation axis of the Terfenol-D,[14] we get

$$\vec{f}_{\mathrm{MS}}(\vec{r}, t, \vec{B}) = \vec{B}(t) \cdot \cos\theta \cdot \frac{\partial \alpha_{33}^B(\vec{r})}{\partial \vec{x}}. \tag{10}$$

Assuming the magnetic field to be applied at a single frequency $\vec{B}(t) = \vec{B}_0 \cdot e^{i\omega_{sig}t}$ and along the main magnetostrictive axis ($\cos\theta = 1$), the above equation reads in frequency space:

$$\vec{f}_{\mathrm{MS}}(\vec{r}, \omega, \vec{B}_0) = B_0 \cdot \frac{\partial \alpha_{33}^B(\vec{r})}{\partial \vec{x}} \cdot \delta(\omega - \omega_{sig}). \tag{11}$$

The magnetostrictive coefficient α_{33}^B is only non-zero in the central Terfenol-D disk with radius $\tilde{R}$ that is described by the Heaviside step function $\Theta(\tilde{R} - r)$, and therefore we can calculate the force density at the signal frequency ω_{sig}

$$\alpha_{33}^B(\vec{r}) = \alpha_{33}^B \cdot \Theta(\tilde{R} - r) \Longrightarrow \frac{\partial \alpha_{33}^B(\vec{r})}{\partial \vec{r}} = \alpha_{33}^B \cdot \delta(\tilde{R} - r)$$

$$\Longrightarrow \vec{f}_{\mathrm{MS}}(\vec{r}, \omega_{\mathrm{sig}}, \vec{B}_0) = B_0 \frac{\partial \alpha(\vec{r})}{\partial \vec{r}} \frac{\partial \vec{r}}{\partial \vec{x}} \hat{e}_x = B_0 \alpha_{33}^B \delta(\tilde{R} - r) \cos\beta \hat{e}_x, \tag{12}$$

where we use cylindrical coordinates ($r = |\vec{r}|, \beta = \arctan\left(\frac{x}{y}\right), h = z$). The magnetostrictive force density is therefore zero everywhere except on the perimeter of the Terfenol-D disk, described by a $\delta-$function. Naturally, it always points in the direction of the applied magnetic field and it is proportional to its amplitude B_0 and the magnetostrictive stress coefficient α_{33}^B. The dependence on the angle β stems from the geometry of the Terfenol-D disk. Inserting $\vec{f}_{\mathrm{MS}}$ and $\vec{\Psi}_q(\vec{r})$ into Eq. (6) yields the magnetic actuation constant

$$\begin{aligned}
c_{act} &= H \cdot \int_0^\infty \int_0^{2\pi} \alpha_{33}^B \delta(\tilde{R} - r)\cos(\beta)(\hat{e}_x \cdot \vec{r})\frac{\sqrt{2}}{R} d\beta r dr \\
&= \frac{\sqrt{2}H\alpha_{33}^B}{R} \int_0^\infty \int_0^{2\pi} \delta(\tilde{R} - r)r^2 \cos(\beta)(\hat{e}_x \cdot \hat{e}_r) \\
&= \frac{\sqrt{2}H\tilde{R}^2\alpha_{33}^B}{R} \cdot \alpha_{33}^B \cdot \int_0^{2\pi} \cos^2(\beta)d\beta \\
&= \frac{\pi\sqrt{2}H\tilde{R}^2\alpha_{33}^B}{R} = 302\mu m^2 \cdot \alpha_{33}^B,
\end{aligned} \tag{13}$$

where we have used the fact that $(\hat{e}_x \cdot \hat{e}_r) = \cos\beta$. The result can be interpreted as the Terfenol-D disk applying a field dependent pressure determined by the magnetostriction coefficient over an effective area of $302 \ \mu\mathrm{m}^2$.

In order to calculate the magnetostrictive stress coefficient α_{33}^B from a magnetostrictive strain coefficient d_{33}^H that we know from literature,[27, 28] we need to determine the relationship between the external magnetic flux density B_{ext}, which we aim to detect, and field strength inside the material H_{in}. As we assume the magnetic field to be in parallel with the Terfenol-D disk, we can use the demagnetization factor $N = 0$ for a flat disk.[29] In this case, B_{ext} and H_{in} are related simply by the magnetic permeability of free space

$$H_{\mathrm{in}} = H_{\mathrm{ext}} = \mu_0^{-1} B_{\mathrm{ext}}. \tag{14}$$

The equivalent relation follows between the magnetostrictive stress coefficients α_{33}^B and α_{33}^H, which quantify the response of Terfenol-D on applied magnetic flux densities B and magnetic field strengths H. Furthermore, the magnetostrictive stress- and strain coefficients are connected by the Young modulus E of Terfenol-D

$$\alpha_{33}^B = \mu_0^{-1}\alpha_{33}^H = \mu_0^{-1}Ed_{33}^H. \tag{15}$$

We use the value $d_{33}^H = 1.7$ ppm/Oe from Ref.,[28] which is a rather conservative estimation (compare Ref.[27]). Using $E=30$ GPa and $\mu_0 = 10^{-4}$ T/Oe. We get from the above equation $\alpha_{33}^B = 5 \cdot 10^8$ Pa/T. Inserting this in Eq. 13 finally yields

$$c_{\text{act}} = 0.19 \frac{N}{T}. \tag{16}$$

2.4 Predicted sensitivity and discussion

The minimal detectable field $B_{\min}$ as a function of frequency for a measurement time of one second calculated from Eq. (5) is shown in Fig. 2. In the shot noise limited case (solid red line), the Brownian noise (dashed blue line) dominates over the measurement noise from DC to about 15 MHz, allowing a sensitivity of about 750 fT/$\sqrt{\text{Hz}}$. For frequencies much higher than the mechanical resonance frequency, the susceptibility of the
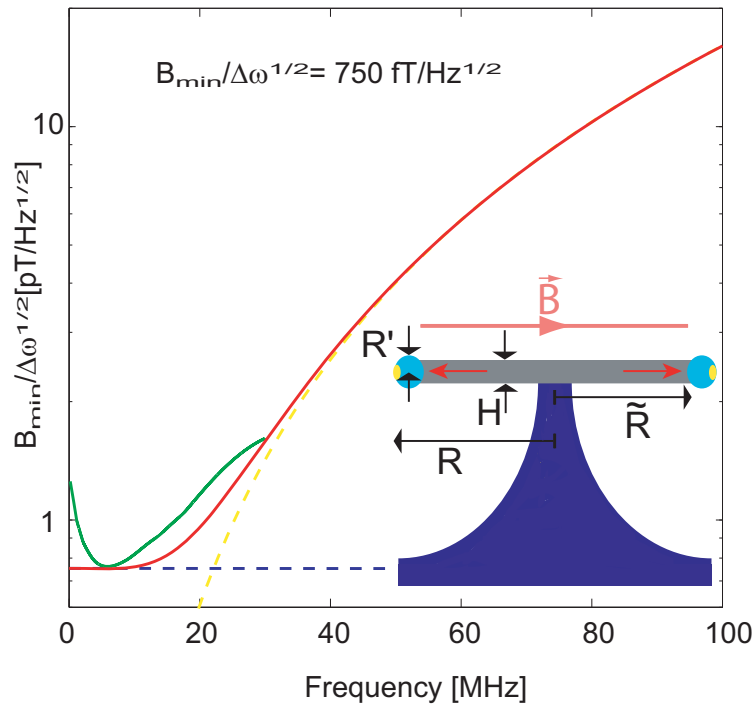

Figure 2. (color online) B-field sensitivity of a toroidal WGM based magnetometer. Dashed blue line (partly hidden by inset): Detection limit due to Brownian noise. Dashed yellow line: Detection limit due to laser shot noise. At the mechanical resonance frequency of 5.6 MHz the shot noise detection limit would be as low as 100 aT/$\sqrt{\text{Hz}}$ (not shown in figure). Solid red line: Magnetic field detection limited by Brownian noise and laser shot noise. The solid green line takes into account thermorefractive noise, Brownian noise and laser shot noise. Inset: Cross-section of the toroidal WGM resonator consisting of a Terfenol-D disc (in gray) surrounded by an optical silica resonator (light blue, optical field yellow). Red arrows represent the direction of the magnetostrictive force.

oscillator decreases as $1/\omega$ and thus at frequencies above 15 MHz, the laser shot noise (dashed yellow line) dominates and the sensitivity decreases approximately as the mechanical susceptibility. If the measurement is limited by thermorefractive noise (solid green line), the sensitivity below 30 MHz is degraded by a factor of about two, except for a frequency band of a few megahertz around the mechanical resonance frequency, where the Brownian noise dominates over the thermorefractive noise and again a peak sensitivity of 750 fT/$\sqrt{\text{Hz}}$ is achieved. We used experimentally measured values for the thermorefractive noise spectrum from Ref.[22]

It should be noted that the calculated sensitivity is a conservative estimation, as by optimized heat-treatment and applied prestress on the Terfenol-D, and by choosing an ideal bias magnetic field the magnetostrictive strain

coefficient d_{33}^H can reach values of up to 25 ppm/Oe, potentially increasing the achievable sensitivity by a factor of 15. We have also investigated other optomechanical systems, in particular microscale Fabry-Perot resonators[30] and photonic-crystal cavities,[31] as potential magnetic field sensors.[18] However, the toroidal WGM magnetometer shows the best predicted sensitivity its geometry allows for an efficient coupling of the magnetostrictive stress to the mechanical radial breathing mode.

3. CONCLUSION

Calculations based on a finite element model and the theory developed for this purpose[19] predict it may be possible to achieve sensitivities in the high $\text{fT}/\sqrt{\text{Hz}}$ range with a sensor based on a toroidal whispering-gallery-mode cavity and utilizing the magnetostrictive alloy Terfenol-D. If fabrication related challenges can be mastered, the suggested sensor could potentially combine high sensitivity with microscale resolution and 3-D field imaging capability due to its small geometric size and the ability to be fabricated in a dense 2-dimensional array on a silicon chip.[36] It could be very versatile, having a number of uses in imaging, especially in the medical field. The ability to operate at room temperature and in relatively high bias fields of up to ~ 0.8 Tesla together with the uncomplicated optical readout could make it a useful tool, in particular for portable applications.

ACKNOWLEDGMENTS

REFERENCES

[1] Edelstein, A., "Advances in magnetometry," J. Phys.-Condes. Matter 19, 28 (2007).

[2] Romalis, M. V., and Dang, H. B., "Atomic magnetometers for materials characterization," Materials Today 14, 258 (2011).

[3] Sawicki, M., Stefanowicz, W. and Ney, A., "Sensitive SQUID magnetometry for studying nanomagnetism," Semicon. Sci. Tech. 26, 064006 (2011).

[4] Dang, H. B., Maloof, A. C. and Romalis, M. V., "Ultrahigh sensitivity magnetic field and magnetization measurements with an atomic magnetometer," Appl. Phys. Lett. 97, 151110 (2010).

[5] Allred, J. C., Lyman, R. N., Kornack, W. and Romalis, M.V., "High-Sensitivity Atomic Magnetometer Unaffected by Spin-Exchange Relaxation," Phys. Rev. Lett. 89, 130801 (2002).

[6] Maser, D. et al., "Detection of a single cobalt microparticle with a microfabricated atomic magnetometer," Rev. Sci. Inst. 82, 086112 (2011).

[7] Budker, D. and Romalis, M., "Optical magnetometry," Nat. Phys. 3, 227 (2007).

[8] Balasubramanian, G. et al., "Ultralong spin coherence time in isotopically engineered diamond," Nat. Mat. 8, 383 (2009).

[9] Maze, J. R. et al., "Nanoscale magnetic sensing with an individual electronic spin in diamond," Nature 455, 644-647 (2008).

[10] Grinolds, M. S. et al., "Quantum control of proximal spins using nanoscale magnetic resonance imaging," Nat. Phys. 7, 687 (2011).

[11] Pham, L. M. et al., "Magnetic field imaging with nitrogen-vacancy ensembles," New J. Phys. 13 (2011).

[12] Schoenfeld, R. S. and Harneit, W., "Real Time Magnetic Field Sensing and Imaging Using a Single Spin in Diamond," Phys. Rev. Lett. 106, 030802 (2011).

[13] Bucholtz, F., Dagenais, D. M. and Koo, K. P., "High-frequency fibre-optic magnetometer with 70 $fT/\sqrt{Hz}$ resolution, "Elec. Lett. 25, 1719 (1989).

[14] Olabi, A. G. and Grunwald, A., "Design and application of magnetostrictive materials," Materials & Design 29, 469-483 (2008).

[15] Shuxiang, D., Jie-Fang, L. and Viehland, D., "Ultrahigh magnetic field sensitivity in laminates of TERFENOL-D and $Pb(Mg_{\frac{1}{3}}Nb_{\frac{2}{3}})O_3$-$PbTiO_3$ crystals," App. Phys. Lett. 83, 2265-2267 (2003).

[16] Quintero, S. M. M., Braga,A. M. B., Weber,H. I., Bruno, A. C. and Araujo, J. F. D. F., "A Magnetostrictive Composite-Fiber Bragg Grating Sensor'" Sensors 10, 8119-8128 (2010).

[17] Osiander, R., Ecelberger, S. A., Givens, R. B., Wickenden, D. K., Murphy, J. C. and Kistenmacher,T. J., "A microelectromechanical-based magnetostrictive magnetometer," App. Phys. Lett. 69, 2930-2931 (1996).

[18] Forstner, S., Prams, S., Knittel, J., van Ooijen, E.D., Swaim, J.D., Harris, G.I., Szorkovszky, A., Bowen, W.P. and Rubinsztein-Dunlop, H., Cavity Optomechanical Magnetometer, Phys. Rev. Lett. 108, 120801 (2012).

[19] Knittel, J., Forstner, S., Swaim, J. D., Rubinsztein-Dunlop, H. and Bowen, W. P. Sensitivity of cavity optomechanical field sensors, Proc. SPIE 8351, 83510H (2012).

[20] Schliesser, A. and Kippenberg, T. J., "Cavity optomechanics with whispering-gallery mode optical micro-resonators," Adv. Atom. Mol. Opt. Phys. 58 207-323 (2010).

[21] Schliesser, A., "Cavity Optomechanics and Optical Frequency Comb Generation with Silica Whispering-Gallery-Mode Microresonators," PhD thesis, Ludwig-Maximilians-Universität (2009).

[22] Schliesser, A., Anetsberger, G., Riviere, R. , Arcizet, O. and Kippenberg,T. J., "High-sensitivity monitoring of micromechanical vibration using optical whispering gallery mode resonators," New J. Phys. 10, 095015 (2008).

[23] Gorodetsky, M. L. and Grudinin, I. S., "Fundamental thermal fluctuations in microspheres," J. Opt. Soc. Am. B 21, 697-705 (2004).

[24] Greenwood, N. N. and Earnshaw, A., [Chemistry of the Elements], Oxford Pergamon (1984).

[25] Cleland, A. N., [Foundations of Nanomechanics], Springer (1965).

[26] Engdahl, G., [Handbook of giant magnetostrictive materials], Academic Press, London (2000).

[27] Verhoeven, J.D., Gibson, E.D., McMasters, O.D. and Ostenson, J.E., "Directional Solidification and Heat Treatment of Terfenol-D Magnetostrictive Materials," Metal. and Mat. Trans. A 21(8), 2249-2255 (1990).

[28] Kellogg, R. and Flatau, A., "Blocked force investigation of a Terfenol-D transducer," Proc. SPIE 3329, 3668-19 (1999).

[29] S. Blundell., [Magnetism in condensed matter], Oxford University Press (2001).

[30] Antoni, T. et al. "Deformable two-dimensional photonic crystal slab for cavity optomechanics," Opt. Lett. 36(17), 3434-3436 (2011).

[31] Alegre, T. P. M., Perahia, R. and Painter, O., "Optomechanical zipper cavity lasers: theoretical analysis of tuning range and stability," Opt. Exp. 18(8), 7872-7885 (2010).

[32] Anetsberger, G., Riviere, R., Schliesser, A., Arcizet, O. and Kippenberg, T. J. "Ultralow-dissipation optomechanical resonators on a chip," Nat. Phot. 2, 627-633 (2008).

[33] Martelli, C., Olivero, P., Canning, J., Groothoff, N., Gibson, B. and Huntington, S., "Micromachining structured optical fibers using focused ion beam milling," Opt. Lett. 32(11), 1575-1577 (2007).

[34] Soltani, M., Yegnanarayanan, S. and Adibi, A., "Ultra-high Q planar silicon microdisk resonators for chip-scale silicon photonics," Opt. Exp. 15(8), 4694-4704 (2007).

[35] Loveless, M., Guruswamy, S. and Shield, J. E., "Crystallization behavoiur of amorphous Terfenol-D thin films," IEEE Trans. Magn. 33 (5), 3937-3939 (1997).

[36] Xia, F., Sekaric, L. and Vlasov, Y., "Ultracompact optical buffers on a silicon chip," Nat. Phot. 1, 65-71 (2007).